Coherent population trapping in cesium: Dark lines and coherent microwave emission

Jacques Vanier,* Aldo Godone, and Filippo Levi
Istituto Elettrotecnico Nazionale, Galileo Ferraris, Torino, 10039, Italy
(Received 27 April 1998)

The phenomenon of coherent population trapping in alkali-metal atoms is analyzed by means of a perturbation approach. Closed form transparent solutions are obtained for the coherences existing within the system and the populations of the ground levels and of the excited state. The presence of dark lines and coherent microwave emission from the ground state are made explicit. Experimental results that confirm the theoretical calculations are reported for the case of cesium in a buffer gas. Conclusions are drawn in connection with the application of coherent population trapping to the field of atomic frequency standards.
[S1050-2947(98)12709-9]

PACS number(s): 32.80.Wr, 32.10.Fn, 32.30.Bv, 32.70.Jz

I. INTRODUCTION

The coupling of two ground states to a common excited state by means of two coherent radiations leads to interference effects in the excitation process, a phenomenon that has been called coherent population trapping (CPT). Its observation was first reported by Alzetta *et al.* [1]. A theoretical analysis of the phenomenon was developed by Orriols [2] and a review of its application in laser spectroscopy has been published recently by Arimondo [3]. The phenomenon has been proposed for applications in the field of atom cooling [4], magnetometry [5], lasing without inversion [6], and atomic frequency standards [7–9].

The phenomenon is readily observed in alkali-metal atoms when coupling of the two ground-state hyperfine levels to the P state is accomplished by means of two laser radiations via a so-called Λ scheme. When the frequency of the two laser radiations is resonant with the transitions, an interference phenomenon takes place in the excitation and the atoms can no longer absorb energy from the lasers. Scattered radiation from the atoms is greatly reduced and the interference leads to the presence of a dark line in the fluorescence spectrum. The phenomenon creates also a strong coherence, coupling the two ground-state hyperfine levels, but does not affect their population, which remains in thermal equilibrium. This coherence creates an oscillating magnetization that leads to the emission of coherent microwave radiation [10].

The dark line can be observed directly in cells containing the alkali atoms with or without a buffer gas. In the absence of a buffer gas the effect takes place over a width controlled mainly by the atom transit time across the laser beams. This may lead to a linewidth of the order of several hundred kHz depending on the actual physical arrangement [11]. When a buffer gas is used this width is greatly reduced due to the Dicke effect [12]. It is mainly controlled by ground state relaxation and laser power broadening. This last situation is of great interest since it leads to linewidths of the same magnitude as those obtained in the observation of magnetic resonance lines by means of standard radio frequency techniques in alkali vapors. On the other hand, the emission of coherent microwave radiation may be observed in a microwave cavity tuned to the frequency of the oscillating magnetization.

The present study is concerned mainly with cesium in various buffer gases although most of the analysis can be applied to other alkali atoms. First, a theoretical analysis of CPT using a simple perturbation approach is developed. Although exact solutions of the phenomenon have been obtained by Orriols [2], the resulting expressions are not transparent and do not lead to easy interpretation; numerical solutions are required to interpret the experimental data. In the present perturbation analysis, closed form transparent approximate solutions are derived for the populations and the coherences in the limit when the laser Rabi frequencies are smaller than the decay rate of the P state. A description of the experimental arrangement used to observe the dark line and the coherent microwave emission is given. Experimental results on important physical effects and parameters are reported and confirm the theoretical predictions. Finally, conclusions are drawn on the possible use of the phenomenon in the implementation of practical frequency standards.

II. THEORY

The energy level scheme used in the analysis is shown in Fig. 1. The two lower levels μ' and μ represent two Zeeman levels within the respective $F=4$ and $F=3$ hyperfine levels of the cesium ground state. The level m represents either the $P_{1/2}$ or $P_{3/2}$ states. It is assumed that these levels are decoupled from the other states. This assumption is validated by the type of excitation used. The lasers couple the ground state only to either of the P states. Within the ground state we will be able, through appropriate means such as the application of a magnetic field or excitation with coherent radiation, to decouple the Zeeman levels in order to allow the observation of isolated pairs of these levels.

The laser fields are written as

$$\mathbf{E}(\omega_n,t,z)=E_{on}\mathbf{e}_\lambda\cos(\omega_n t+\mathbf{k}_n\cdot\mathbf{r}) \tag{1}$$

and we define the optical Rabi frequency as

$$\omega_{nij}=-(E_{on}/\hbar)\langle i|e\mathbf{r}\cdot\mathbf{e}_\lambda|j\rangle, \tag{2}$$

*Present address: Département de Physique, Université de Montréal, Montréal, Québec, Canada.

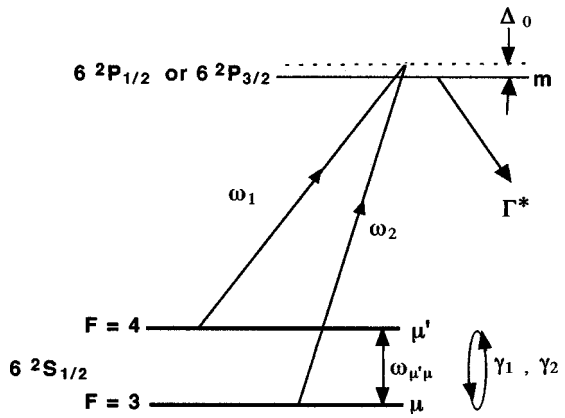

FIG. 1. Energy levels manifold considered in the analysis. ω_1 and ω_2 are the laser angular frequencies; $\omega_{\mu'\mu}/2\pi$ is the hyperfine frequency (9 192 631 770 Hz) shifted by various perturbations described in the text; γ_1 and γ_2 are the ground-state relaxation rates of the populations and of the coherence respectively; Γ^* is the decay rate from the excited state m to the ground-state levels; Δ_0 is the lasers detuning from optical resonance.

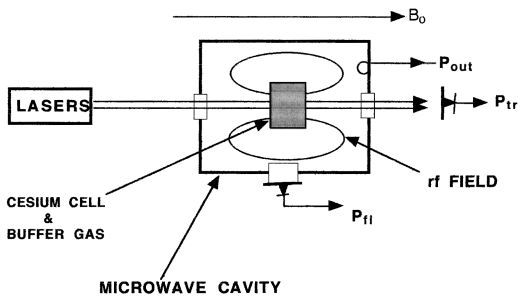

FIG. 2. Schematic illustration of the setup used for the theoretical analysis. The cavity operates in the TE_{011} mode. The two laser radiations are assumed colinear. P_{tr} and P_{fl} are the transmitted and the fluorescence optical powers, respectively, and P_{out} is the microwave cavity power output.

where $\mathbf{e}_\lambda$ is the polarization vector, $\hbar$ is Planck constant over 2π, $\mathbf{k}_n$ is the wave vector for the field at frequency ω_n ($n=1,2$).

In part of the analysis we assume the presence of a rf field along the z direction, at the frequency ω_{rf}, close to the hyperfine frequency,

$$\mathbf{B}_{rf}(r,t)=\mathbf{z}B_z(r)\sin\,\omega_{rf}t, \tag{3}$$

and we define the associated Rabi frequency as

$$b(r)=-\mu_z B_z/\hbar, \tag{4}$$

where μ_z is the magnetic dipole moment of the hyperfine transition; $\mu_z=\mu_B$ (Bohr magneton) for the $m_F=0\rightarrow m_F=0$. This field may be created by means of a cavity as illustrated in Fig. 2.

We make the following assumptions. (i) the population of the ground levels tends to equilibrium at the rate γ_1; relaxation of the cesium atoms is caused mainly by collisions with the buffer gas atoms or molecules and Cs-Cs spin exchange collisions; we neglect the small Boltzmann difference of populations between the ground-state levels. (ii) in the absence of applied fields, coherence in the ground state tends to zero at the rate γ_2; the source of relaxation is essentially the same as in the case of γ_1. (iii) decay from the excited state m takes place at the rates $\Gamma^*_{m\mu}$ and $\Gamma^*_{m\mu'}$, which include both the effect of spontaneous emission and of relaxation by collisions with the buffer gas atoms or molecules; in our case $\Gamma^*_{m\mu}=\Gamma^*_{m\mu'}=\Gamma^*/2$.

The evolution of the atomic system is analyzed in the ensemble-averaged density matrix formalism [13]. We obtain six equations, three for the populations $\rho_{\mu\mu}$, $\rho_{\mu'\mu'}$, ρ_{mm}, and three for the coherences $\rho_{\mu\mu'}$, $\rho_{\mu m}$, and $\rho_{\mu' m}$. We make the long-wavelength approximation and we assume solutions of the form

$$\rho_{\mu' m}=\delta_{\mu' m}e^{i\omega_2 t}, \tag{5}$$

$$\rho_{\mu m}=\delta_{\mu m}e^{i\omega_1 t}, \tag{6}$$

$$\rho_{\mu\mu'}=\delta_{\mu\mu'}e^{i(\omega_1-\omega_2)t}. \tag{7}$$

The resonance frequencies are affected by the Doppler effect. However, the Λ excitation process used in the present analysis is velocity selective since the two laser fields interact simultaneously only with a given group of atoms having velocity v within the range dv. The spread of velocities in interaction is determined by the width of the laser spectrum and the excited-state lifetime. Consequently, we assume that the lasers are in interaction with a specific group of atoms with resonance angular frequencies $\omega_{m\mu}$, $\omega_{m\mu'}$, and $\omega_{\mu'\mu}$, which include a Doppler shift.

We make the rotating wave approximation and keep only the resonant terms. We obtain for a given group of velocities the following set of rate equations:

$$\frac{d}{dt}\rho_{mm}=\omega_{1m\mu}\mathrm{Im}\delta_{\mu m}+\omega_{2m\mu'}\mathrm{Im}\delta_{\mu' m}-\Gamma^*\rho_{mm}, \tag{8}$$

$$\frac{d}{dt}\rho_{\mu'\mu'}=\mathrm{Im}\,ib\,\delta_{\mu\mu'}-\omega_{2m\mu'}\mathrm{Im}\delta_{\mu' m}+\Gamma^*_{m\mu'}\rho_{mm}-(\gamma_1/2)(\rho_{\mu'\mu'}-\rho_{\mu\mu}), \tag{9}$$

$$\frac{d}{dt}\rho_{\mu\mu}=-\mathrm{Im}\,ib\,\delta_{\mu\mu'}-\omega_{1m\mu}\mathrm{Im}\delta_{\mu m}+\Gamma^*_{m\mu}\rho_{mm}-(\gamma_1/2)(\rho_{\mu\mu}-\rho_{\mu'\mu'}), \tag{10}$$

$$\frac{d}{dt}\delta_{\mu\mu'}+\{i(\omega_{21}-\omega_{\mu'\mu})+\gamma_2\}\delta_{\mu\mu'}=-(b/2)(\rho_{\mu'\mu'}-\rho_{\mu\mu})-i(\omega_{1\mu m}/2)\delta_{m\mu'}+i(\omega_{2m\mu'}/2)\delta_{\mu m}, \tag{11}$$

$$\frac{d}{dt}\,\delta_{\mu m}+\{i(\omega_1-\omega_{m\mu})+\Gamma^*/2\}\delta_{\mu m}=-i(\omega_{1\mu m}/2)(\rho_{mm}-\rho_{\mu\mu})-(b/2)\,\delta_{\mu' m}+i(\omega_{2\mu' m}/2)\,\delta_{\mu\mu'}, \tag{12}$$

$$\frac{d}{dt}\,\delta_{\mu' m}+\{i(\omega_2-\omega_{m\mu'})+\Gamma^*/2\}\delta_{\mu' m}=-i(\omega_{2\mu' m}/2)(\rho_{mm}-\rho_{\mu'\mu'})-(b/2)\,\delta_{\mu m}+i(\omega_{1\mu m}/2)\,\delta_{\mu'\mu}, \tag{13}$$

where Γ^* is the total decay rate from the excited state m to the two ground levels μ' and μ, $\omega_{21}=\omega_2-\omega_1$, and Im means imaginary part. We recall that the δ_{ij}'s are complex conjugates of the δ_{ji}'s. The above set of equations is sufficient to describe the system. A large number of theoretical works has been done on the solution of this set of equations or related ones in specific situations [14]. Orriols [2] has formulated a rather complete solution in the case in which the rf field B_z is equal to zero. The solution obtained, however, is not transparent to easy interpretation and a numerical analysis with graphical solutions is required to interpret the results. It provides nevertheless an extremely useful basis for an understanding of the physical processes taking place and gives the relative size of the matrix elements in standard situations encountered in practice. In particular, for the case $b=0$, and when the lasers have equal amplitudes and their frequency difference is close to the hyperfine frequency, it is found that (1) the populations $\rho_{\mu\mu}$ and $\rho_{\mu'\mu'}$ of the ground levels remain equal; (2) the population ρ_{mm} of the excited state m is much smaller than that of the ground state and tends to zero at high laser intensity; (3) the coherence $\delta_{\mu\mu'}$ in the ground state is nearly $-\frac{1}{2}$ and has a value only over a narrow range of the laser frequency difference; this range is of the order of γ_2 and is a function, to a certain extent, of the laser interaction; (4) the coherences $\delta_{\mu m}$ and $\delta_{\mu' m}$, coupling the ground levels to the excited P state are very small relative to $\delta_{\mu\mu'}$.

Based on these conclusions a perturbation calculation is developed in order to obtain closed form analytical expressions for the coherences and populations, expressions that lead to direct easy interpretation of experimental data. We solve the system of equations for both cases when the rf field is either present or absent.

A. Dark lines

In this part of the analysis the rf field B_z is set equal to zero. This can be done by removing conceptually the cavity in Fig. 2. In that case the Rabi frequency b is zero in Eqs. (9)–(13). For simplicity we assume that the two lasers amplitude are equal, making $\omega_{1\mu m}=\omega_{2\mu' m}$ and we call them ω_R. We first solve for $\delta_{m\mu'}$ and $\delta_{\mu m}$ in zero order, that is, $\rho_{mm}=0$, and near the center of the resonance where $(\omega_1-\omega_{m\mu})^2\ll(\Gamma^*/2)^2$ and $(\omega_2-\omega_{m\mu'})^2\ll(\Gamma^*/2)^2$. In steady state, we obtain

$$\delta_{\mu m}=i(\omega_R/\Gamma^*)(\rho_{\mu\mu}+\delta_{\mu\mu'}), \tag{14}$$

$$\delta_{m\mu'}=-i(\omega_R/\Gamma^*)(\rho_{\mu'\mu'}+\delta_{\mu\mu'}). \tag{15}$$

We replace these expressions back into the steady-state equation for $\delta_{\mu\mu'}$,

$$\delta_{\mu\mu'}[\gamma_2+i(\omega_{21}-\omega_{\mu'\mu})]=i(\omega_R/2)(\delta_{\mu m}-\delta_{m\mu'}), \tag{16}$$

to obtain a first-order approximation. We use the notation

$$\delta_{ij}=\delta^r_{ij}+i\,\delta^i_{ij} \tag{17}$$

and we obtain

$$\delta^r_{\mu\mu'}=-\frac{\omega_R^2/2\Gamma^*(\gamma_2+\omega_R^2/\Gamma^*)}{(\gamma_2+\omega_R^2/\Gamma^*)^2+(\omega_{21}-\omega_{\mu'\mu})^2}, \tag{18}$$

$$\delta^i_{\mu\mu'}=\frac{\omega_R^2/2\Gamma^*(\omega_{21}-\omega_{\mu'\mu})}{(\gamma_2+\omega_R^2/\Gamma^*)^2+(\omega_{21}-\omega_{\mu'\mu})^2}, \tag{19}$$

where

$$\omega_{21}=\omega_2-\omega_1. \tag{20}$$

Equations (12) and (13) are solved for conditions close to optical resonance. Using the same notation as above we obtain

$$\delta^i_{\mu m}=\frac{1}{4}\,\frac{\omega_R\Gamma^*/2}{(\Gamma^*/2)^2+(\omega_1-\omega_{m\mu})^2}\,(1+2\,\delta^r_{\mu\mu'}), \tag{21}$$

$$\delta^r_{\mu m}=\frac{1}{4}\,\frac{\omega_R}{(\Gamma^*/2)^2+(\omega_1-\omega_{m\mu})^2}\,[(\omega_1-\omega_{m\mu})-\Gamma^*\delta^i_{\mu\mu'}], \tag{22}$$

$$\delta^i_{\mu' m}=\frac{1}{4}\,\frac{\omega_R\Gamma^*/2}{(\Gamma^*/2)^2+(\omega_2-\omega_{m\mu'})^2}\,(1+2\,\delta^r_{\mu\mu'}), \tag{23}$$

$$\delta^r_{\mu' m}=\frac{1}{4}\,\frac{\omega_R}{(\Gamma^*/2)^2+(\omega_2-\omega_{m\mu'})^2}\,[(\omega_2-\omega_{m\mu'})+\Gamma^*\delta^i_{\mu\mu'}]. \tag{24}$$

The population of level m is given by

$$\rho_{mm}=(\omega_R/\Gamma^*)(\mathrm{Im}\,\delta_{\mu m}+\mathrm{Im}\,\delta_{\mu' m}). \tag{25}$$

Using the expressions just found above for $\delta_{\mu m}$ and $\delta_{\mu' m}$, we obtain

$$\rho_{mm}=\frac{\omega_R^2}{8}\left[\frac{1}{(\Gamma^*/2)^2+(\omega_1-\omega_{m\mu})^2}+\frac{1}{(\Gamma^*/2)^2+(\omega_2-\omega_{m\mu'})^2}\right](1+2\,\delta^r_{\mu\mu'}) \tag{26}$$

with the condition

$$\rho_{\mu\mu}=\rho_{\mu'\mu'}\sim\tfrac{1}{2}. \tag{27}$$

The term ω_R^2/Γ^* that appears in Eqs. (18) and (19) acts as a pumping mechanism; it creates a hyperfine coherence and an associated oscillating magnetization as will be shown below. It also leaves the ground-state populations unaltered. We call it the transverse pumping rate and to simplify notation we define $\Gamma' = \omega_R^2/\Gamma^*$.

It is recalled that these expressions apply for lasers closely tuned to the resonance frequencies $\omega_{m\mu}$ and $\omega_{m\mu'}$ and to a group of atoms having velocity v_z. The resulting Doppler effect is included in the angular frequencies $\omega_{m\mu}$ and $\omega_{m\mu'}$. Interaction with various groups of atoms at different velocities is realized by varying Δ_0, the detuning of both lasers from the Doppler free resonance frequencies. It is also noted that the interaction takes place over a spread of frequencies (or velocities) that is a function of the atom lifetime in the P state and of the lasers spectral width. In the expression for $\delta_{\mu\mu'}$, the hyperfine angular frequency is shifted by the Doppler effect. The resonant angular frequency $\omega_{\mu'\mu}$ is equal to $\omega_{\rm hf}+(k_1-k_2)v_z$. One thus expects a hyperfine resonance affected by Doppler broadening. In the presence of a buffer gas, which is the case studied here, the Doppler effect is cancelled through the Dicke effect [12,7]. The effect of collisions with the buffer gas atoms is taken into account in the relaxation rates γ_1 and γ_2 and a redefinition of the hyperfine frequency as will be done below.

In particular, these expressions show that for $\Gamma' \gg \gamma_2$, a condition that can be satisfied without causing saturation of the optical transitions, $\delta_{\mu\mu'}$ is real at resonance and tends to $-\frac{1}{2}$. Furthermore $\delta_{\mu m}$ and $\delta_{\mu' m}$ are very small of the order of $10^{-2}-10^{-3}$. It is finally observed that $\rho_{\mu\mu}$ and $\rho_{\mu'\mu'}$ are equal with a value close to $\frac{1}{2}$. The phenomenon has been called coherent population trapping. The effects just mentioned reinforce the validity of the approximation made earlier in connection to the population of the excited state and we expect that the expressions obtained to be correct over a large range of Γ' as long as optical saturation does not take place.

An interesting practical aspect of these effects is observed either on the fluorescence radiation emitted or the energy absorbed by the ensemble. The total fluorescence power emitted is readily obtained as

$$P_{\rm fl} = \hbar\omega_L \Gamma_{\rm fl} N \rho_{mm} \tag{28}$$

while the power absorbed by a slice of thickness dz is given by

$$dP_{\rm abs} = \hbar\omega_L \Gamma^* n \rho_{mm} dz, \tag{29}$$

where ω_L is the average angular frequency of the two lasers, n is the atomic density. It is assumed that the decay from the excited state to the two ground-state hyperfine levels takes place at the same rate. In Eq. (28), $\Gamma_{\rm fl}$ is the decay rate of the excited state resulting in fluorescence radiation and N is the total number of atoms interacting with the laser field. The value of ρ_{mm} is obtained from Eqs. (18) and (26). Equations (28) and (29) make explicit the presence of a sharp resonance line that may be detected directly on the fluorescence and absorption spectra. This is the so-called dark line. It is observed by scanning the laser frequency difference. It is present over the full Doppler width of the laser interaction although weighed by the Maxwell velocity distribution. The full width at half the height of the dark line is

$$\Delta\omega_{1/2} = 2(\gamma_2 + \omega_R^2/\Gamma^*) \tag{30}$$

and is sensitive to laser power through the optical Rabi frequency ω_R.

B. Coherent microwave emission in a cavity

1. Justification of some approximations to be made

The off-diagonal elements $\rho_{\mu\mu'}$ and $\rho_{\mu'\mu}$ create a magnetization oscillating at the frequency ω_{21}. The expectation value of this magnetization averaged over the ensemble is readily obtained from the following equation [15]:

$$\overline{\langle M_z \rangle} = {\rm Tr}(M_{\rm op}\rho), \tag{31}$$

and is equal to

$$\overline{\langle M_z \rangle} dv = -\tfrac{1}{2} n \mu_B (\rho_{\mu\mu'} + \rho_{\mu'\mu}) dv, \tag{32}$$

where $\rho_{\mu\mu'}$ and $\rho_{\mu'\mu}$ are given by Eq. (7) with $\delta_{\mu\mu'}$ given by Eqs. (18) and (19). Such an oscillating magnetization emits radiation at the frequency ω_{21}. In the cavity illustrated in Fig. 2, the magnetization excites a particular mode and creates a corresponding field. This field reacts back on the atoms and creates an interaction at the hyperfine frequency with an associated Rabi frequency defined by means of Eq. (4). An examination of Eqs. (8)–(13) shows that the rf field affects significantly the populations and the coherence only when $b \sim \Delta\omega_{1/2}$. As will be shown below, this field is very weak in our experimental arrangement, and b does not take a large value. Actually b is found to be of the order of 1 to $30\ {\rm s}^{-1} \ll \Delta\omega_{1/2}$. Consequently, we can consider independently the interactions with the lasers fields and the rf field. The solutions found above for $\delta_{\mu'\mu}$ with $b=0$ thus applies, and we consider by itself the radiating properties of the oscillating magnetization and its effect on the field in the cavity. The effect of the laser power broadening is then taken care of through its effect on $\delta_{\mu'\mu}$ as shown by Eq. (30).

2. Emission of microwave radiation

a. Continuous operation. We first analyze the situation shown in Fig. 2 when the laser radiation is applied continuously. The rf magnetic field **H** created in the cavity may be described by the classical field equation [12]:

$$\ddot{\mathbf{H}}(r,t) + (\omega_c/Q_L)\dot{\mathbf{H}}(r,t) + \omega_c^2 \mathbf{H}(r,t) = -\mathbf{H}_c(r) \int_{V_c} \mathbf{H}_c(r) \cdot \ddot{\mathbf{M}}(r,t) dv, \tag{33}$$

where ω_c is the cavity resonance frequency, Q_L is the cavity loaded quality factor, V_c is the cavity volume, $\mathbf{H}_c$ is the orthonormal cavity mode, and **M** is the magnetization as calculated above. We write **M** and **H** in complex form:

$$\mathbf{H}(r,t) = \{H^{+*}(r)e^{-i\omega_{21}t} + H^+(r)e^{i\omega_{21}t}\}\mathbf{z}, \tag{34}$$

$$\mathbf{M}(r,t) = \{M^{+*}(r)e^{-i\omega_{21}t} + M^+(r)e^{i\omega_{21}t}\}\mathbf{z}, \tag{35}$$

where H^+ and M^+ are complex amplitudes of the field and of the magnetization, respectively. We replace these expressions in Eq. (33) and use only the resonant components. We obtain

$$\mathbf{H}^+(r)=\frac{-iQ_L}{1+i2Q_L(\Delta\omega_c/\omega_{21})}\,\mathbf{H}_c(r)\int_{V_c}\mathbf{H}_c(r)\cdot\mathbf{M}(r)dv, \tag{36}$$

where $\Delta\omega_c$ is the cavity detuning from the laser frequency difference and is equal to $(\omega_c-\omega_{21})$.

The power dissipated in the cavity is given by [15]:

$$P_{\text{diss}}=\frac{\omega_{21}\mu_0}{Q_L}\int_{V_c}\overline{H^2(r,t)}dv \tag{37}$$

where the horizontal bar on H^2 means a time average. We use Eq. (34) for $\mathbf{H}(r,t)$ and we obtain

$$P_{\text{diss}}=\frac{\omega_{21}\mu_0}{Q_L}\,2\int_{V_c}H^{+*}(r)H^+(r)dv. \tag{38}$$

The value of $M^+(r)$ is obtained from Eq. (32) while $\rho_{\mu\mu'}$ is given by Eq. (7). We finally obtain, with $\omega_{21}\sim\omega_{\mu'\mu}$,

$$P_{\text{diss}}=\tfrac{1}{2}\,\frac{N\hbar\omega_{\mu'\mu}k}{1+4Q_L^2(\Delta\omega_c/\omega_{\mu'\mu})}\,(4\delta_{\mu'\mu}\delta_{\mu\mu'}), \tag{39}$$

where k may be interpreted as the number of microwave photons emitted by an atom in one second; it is given by

$$k=\frac{NQ_L\eta'\mu_B^2\mu_0}{\hbar V_a} \tag{40}$$

and η' is the filling factor defined as

$$\eta'=\frac{V_a\langle H_z(r)\rangle_a^2}{V_c\langle H^2(r)\rangle_c}. \tag{41}$$

Here $\langle\ \rangle_a$ means an average over the volume V_a containing the interacting atoms and $\langle\ \rangle_c$ means an average over the cavity volume. In view of possible field inhomogeneities that may exist in the ensemble, Eq. (39), to be exact, applies only to a subensemble of limited volume in which these fields can be considered homogeneous. However, in the experimental arrangement using the microwave cavity the cell is relatively small and, for simplicity, we will assume that the fields are homogeneous over the ensemble.

Using the value of $\delta_{\mu\mu'}$ calculated previously we finally obtain

$$P_{\text{diss}}=\tfrac{1}{2}\,\frac{N\hbar\omega_{\mu'\mu}k}{1+4Q_L^2(\Delta\omega_c/\omega_{\mu'\mu})^2}\,\frac{\Gamma'^2}{(\gamma_2+\Gamma'^2)^2+(\omega_{21}-\omega_{\mu'\mu})^2}. \tag{42}$$

The power coupled out of the cavity by the loop is given by

$$P_{\text{out}}=\{\beta/(1+\beta)\}P_{\text{diss}}, \tag{43}$$

where β is the cavity coupling coefficient. It is readily observed that the ensemble radiates energy at all laser intensities without a threshold and without population inversion. The emission has a Lorentz shape and is maximum at the frequency $\omega_{21}=\omega_{\mu'\mu}$; its width at half-maximum is $(\gamma_2+\Gamma')/\pi$.

b. Transient operation. In this case the laser light is applied under the form of a pulse as shown in Fig. 3. Three regions are identified as (*A*) region of coherence buildup; (*B*) region of steady-state behavior; (*C*) region of coherence decay in the absence of laser light.

Region A. In this region the coherence $\delta_{\mu\mu'}$ builds up at a rate characteristic of the various relaxation rates. It can be calculated from the density matrix rate equations given earlier. We define

$$\delta'=\delta_{m\mu'}-\delta_{\mu m}. \tag{44}$$

As in the previous analysis we neglect the effect of the rf field on the density matrix elements. Equations (11), (12), and (13) can be written as

$$\frac{d}{dt}\,\delta_{\mu\mu'}+\{i\Omega_\mu+\gamma_2\}\delta_{\mu\mu'}=-i(\omega_R/2)\delta', \tag{45}$$

$$\frac{d}{dt}\,\delta'+(\tfrac{1}{2})\{i\Omega_\mu+\Gamma^*\}\delta'=-i(\omega_R/2)-i\omega_R\delta_{\mu\mu'}, \tag{46}$$

where Ω_μ stands for $(\omega_{21}-\omega_{\mu'\mu})$. It is readily observed that the optical coherence δ' responds to a perturbation at a rate of the order of Γ^* while $\delta_{\mu\mu'}$ responds at a rate of the order of γ_2. This means that the optical coherence reaches its

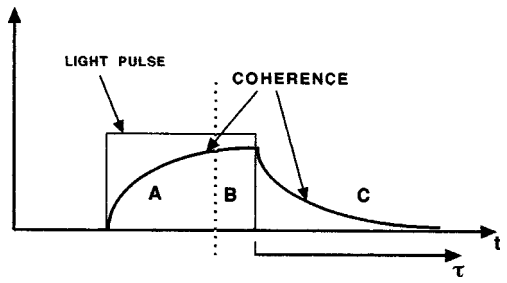

FIG. 3. Identification of the various regions for a laser pulse, as studied in the text. Coherence builds up in region *A*. Steady state is reached in region *B*. In region *C*, the atoms evolve freely at angular frequency $\omega_{\mu'\mu}$ and the coherence decays to zero.

equilibrium value much faster than the rf coherence, Γ^* being of the order of 10^8-10^9, while γ_2 is of the order of 10^2-10^3. Consequently, in order to solve these two equations it is possible to use an approximation in which the optical coherence builds up rapidly while during that time the rf coherence stays at a negligible value. After this buildup the optical coherence follows adiabatically the rf coherence. It is then straightforward to solve the two equations simultaneously. We obtain

$$\delta^r_{\mu\mu'}=-\frac{(\Gamma'/2)(\gamma_2+\Gamma')}{(\gamma_2+\Gamma')^2+\Omega_\mu^2}\left\{1-e^{-(\gamma_2+\Gamma')t}\cos\,\Omega_\mu t+\frac{\Omega_\mu}{(\gamma_2+\Gamma')}\,e^{-(\gamma_2+\Gamma')t}\sin\,\Omega_\mu t\right\}, \tag{47}$$

$$\delta^i_{\mu\mu'}=-\frac{(\Gamma'/2)(\gamma_2+\Gamma')}{(\gamma_2+\Gamma')^2+\Omega_\mu^2}\times\left\{-\frac{\Omega_\mu}{(\gamma_2+\Gamma')}\,(1-e^{-(\gamma_2+\Gamma')t}\cos\,\Omega_\mu t)+e^{-(\gamma_2+\Gamma')t}\sin\,\Omega_\mu t\right\}. \tag{48}$$

The power output, given by Eq. (39) with $\Delta\omega_c=0$, evolves as

$$P_{\rm diss}=\tfrac{1}{2}N\hbar\omega_{12}k\,\frac{\Gamma'^2}{(\gamma_2+\Gamma')^2+\Omega_\mu^2}\times\{1+e^{-2(\gamma_2+\Gamma')t}-2e^{-(\gamma_2+\Gamma')t}\cos\,\Omega_\mu t\}. \tag{49}$$

It is readily observed that the power output is modulated upon buildup at Ω_μ, the frequency difference between ω_{21}, and the atomic frequency $\omega_{\mu'\mu}$. When $\Omega_\mu=0$, the buildup characteristic time is related to the time constant,

$$\tau_p=1/(\gamma_2+\Gamma'). \tag{50}$$

Region B. In this region, equilibrium is reached and the power output is given by Eq. (42).

Region C. In this region, the laser radiation is absent and the atoms evolve freely at their frequency $\omega_{\mu'\mu}$ in the presence of the cavity field. The coherence decays at the rate γ_2 from its equilibrium value at the end of the laser pulse. The power can be obtained directly from Eq. (42) by multiplying the final value by $(\exp-2\gamma_2)$. However, some insight is obtained into the behavior of the ensemble by using a self-consistent approach in which the power given by the atoms is made equal to the power dissipated in the cavity. In order to develop such an approach, we use the rate equations (8), (9), and (10) with the optical Rabi frequency set to zero. We have

$$\frac{d}{dt}\,\rho_{\mu'\mu'}={\rm Im}\;ib\delta_{\mu\mu'}-(\gamma_1/2)(\rho_{\mu'\mu'}-\rho_{\mu\mu}), \tag{51}$$

$$\frac{d}{dt}\,\rho_{\mu\mu}=-{\rm Im}\;ib\delta_{\mu\mu'}-(\gamma_1/2)(\rho_{\mu\mu}-\rho_{\mu'\mu'}), \tag{52}$$

$$\frac{d}{dt}\,\delta_{\mu\mu'}+\{i(\omega_{rf}-\omega_{\mu'\mu})+\gamma_2\}\delta_{\mu\mu'}=-(b/2)(\rho_{\mu'\mu'}-\rho_{\mu\mu}), \tag{53}$$

where ω_{rf} is the frequency of the rf field in the cavity. The problem is reduced to one of magnetic resonance. The solution of this set of equations may be done exactly as in Refs. [16], [17], and [18] as if we were in presence of stimulated emission. The only difference is the condition at the origin after the light pulse. In the case of Ref. [17] the coherence was produced by means of a $\pi/2$ pulse following a light pulse that created an almost complete population inversion. In the present case we have a coherence produced by CPT without population inversion. The power given by the atoms results from transitions from level μ' to level μ and is given by

$$P_{\rm at}=\tfrac{1}{2}\hbar\omega_{\mu'\mu}N\left[\frac{d}{dt}\,\Delta\right]_{\rm rf}, \tag{54}$$

where Δ is the population difference $(\rho_{\mu'\mu'}-\rho_{\mu\mu})$ and where the subscript rf indicates that only transitions caused by the rf field are considered. The power dissipated in the cavity is given by Eq. (37). The system of equations is solved for the case $\omega_{rf}=\omega_{\mu'\mu}$. The coherence at the time origin may be thought of as being produced by a $\pi/2$ pulse applied on an ensemble which had been prepared in a pseudostate of population inversion Δ_p given by

$$\Delta_p=(\rho_{\mu'\mu'}-\rho_{\mu\mu})_p=\frac{(\omega_R^2/\Gamma^*)}{(\gamma_2+\omega_R^2/\Gamma^*)}. \tag{55}$$

The power output is obtained by equating the power given by the atoms to that dissipated in the cavity [Eq. (38)]. It is found that

$$\langle b^2\rangle_b=-k\left[\frac{d}{dt}\,\Delta\right]_{\rm rf}, \tag{56}$$

In the case of a small cell the field may be assumed homogeneous over the ensemble and the Rabi frequency is given by the relation

$$b=-2k\delta^r. \tag{57}$$

This equation provides a simple means of evaluating the amplitude of the field in the cavity. Finally, one obtains

$$P_{\rm diss}=(\tfrac{1}{2})\hbar\omega_{\mu'\mu}Nk\Delta_p^2e^{-2\gamma_2\tau}{\rm sech}^2\{-(\Delta_pk/\gamma_2)\times(1-e^{-2\gamma_2\tau})+\tanh^{-1}(\cos\,\theta_1)\}, \tag{58}$$

where k is given by Eq. (40), and where θ_1 is the phase angle or tipping of the magnetization. In the case of CPT the populations of the two ground levels are equal at the end of the light pulse. This situation is equivalent to the one that would be created in an ensemble of atoms whose ground state populations had been inverted and whose difference of population would be given by Eq. (54) and then submitted to a $\pi/2$ pulse.

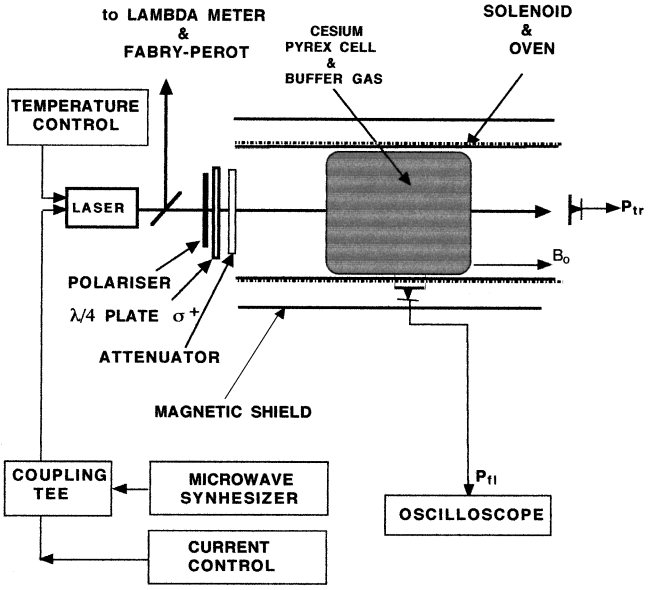

FIG. 4. Experimental arrangement used to observe the dark line. The Fabry-Perot interferometer and the λ meter are not shown in the figure.

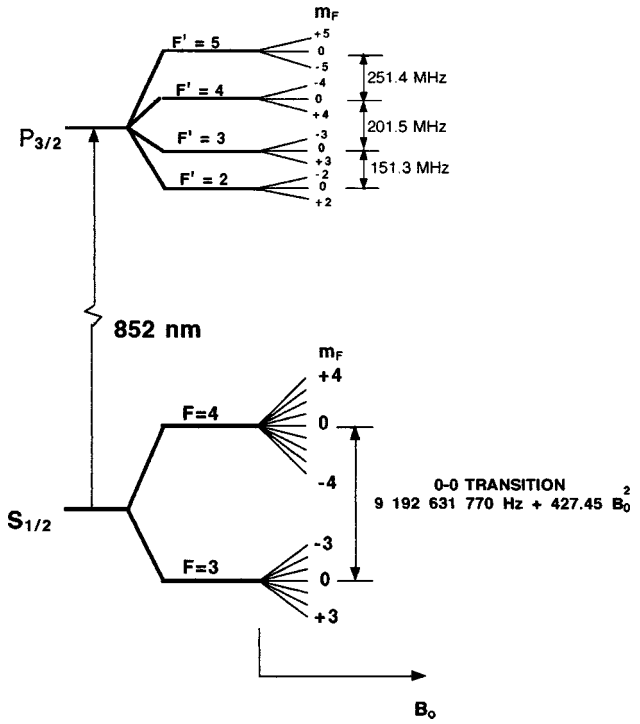

FIG. 5. Lower-energy levels of cesium of interest in the present study.

As will be shown below in connection with the experimental results, k has a value of the order of 20. In that case the term $\mathrm{sech}^2\{\}$ is close to 1. There is thus no radiation damping. The power dissipated in the cavity can then be approximated to

$$P_{\mathrm{diss}}=(\tfrac{1}{2})\hbar\omega_{\mu'\mu}Nk\Delta_p^2 e^{-2\gamma_2\tau}, \tag{59}$$

as was concluded intuitively above.

The power observed at the coupling loop as given by Eq. (43) decays at the rate $2\gamma_2$. A measurement of P_{diss} provides information on the coherence relaxation rate γ_2 while a measurement of the buildup time constant provides information on the transverse pumping rate Γ'.

III. EXPERIMENTAL RESULTS

A. Apparatus

Experiments were done with two different systems. The one shown in Fig. 4 was used for intensive measurements on the dark line. It consists of a laser diode operating at 852 nm (D_2 transition) and a power output of about 15 mW. It is temperature controlled by means of a Peltier element and coupled to an external cavity with a grating for tuning purposes. The injection current of the laser diode is modulated at the angular frequency $\omega_m=\omega_{\mu'\mu}/2$, equal to $2\pi\times4.6$ GHz. The two first sidebands of the resulting spectrum separated by 9.2 GHz provide the two radiations required for coherent population trapping experiments in cesium [19,20]. In our experiments it was possible with some diodes to obtain a frequency modulation index $\mu_f\sim1$. The technique ensures a very high correlation between the two radiations used in the Λ scheme and avoids any divergence encountered when two independent laser beams are used. The rf source is a frequency synthesizer driven by a stable quartz crystal oscillator. The behavior of the laser diode is monitored continuously with a λ meter and a Fabry-Perot interferometer.

The cell is enclosed in a cylinder acting at the same time as a holding structure and an oven for controlling the temperature. Many cylindrical cells 4 cm long and 4 cm in diameter containing cesium and various buffer gases were used. These cells had been fabricated over twenty years ago. The characteristics of these cells had been extensively determined in previous work by means of the intensity optical pumping technique [15] and some of the results were reported in Refs. [21] and [22]. Various tests on frequency shifts and relaxation rates showed that there was no visible degradation of their original characteristics.

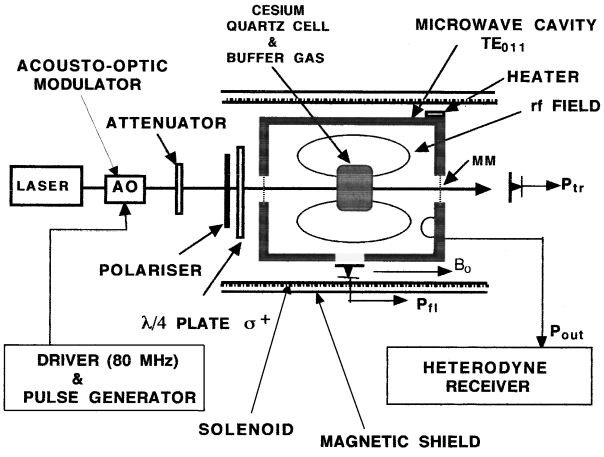

FIG. 6. Experimental arrangement used to observe emission of coherent radiation. MM is a copper metal mesh having a 90% transmission for the laser radiation.

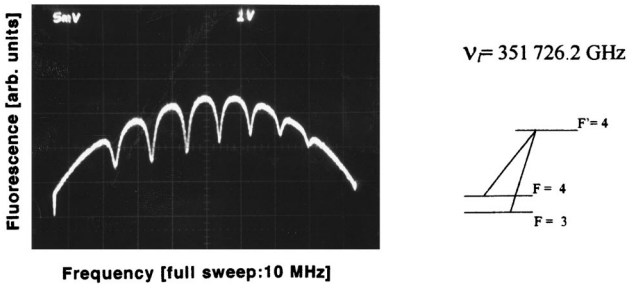

FIG. 7. Dark lines observed in cesium in the case of a cell containing no buffer gas for σ^+ polarization. First sideband laser power density: 1 mw/cm^2. The amplitude of the seven lines, separated by about 850 kHz, corresponds to the size of the transition probabilities calculated from Clebsch-Gordan coefficients as indicated in Table I.

Fluorescence and light transmission are measured with silicon photodetectors placed at right angle to the cell and at the end of the ensemble, respectively. Signal detection is done directly with an oscilloscope. A magnetic field of the order of 400 mG providing the axis of quantization is created by a solenoid. This solenoid is surrounded by a μ-metal magnetic shield to reduce ambient field fluctuations.

In the major part of the experiments to be described we are concerned mainly with $\Delta m_F=0$ transitions and, in particular, with the field independent O-O transition. The lower cesium atom energy levels of interest in the present work are shown in Fig. 5. A straightforward calculation with Clebsch-Gordan coefficients shows that the transition S, F, $m_F=0 \leftrightarrow P$, $F'=F$, $m_F=0$ is not allowed. Consequently, circularly polarized light was used throughout the experiments and this was done with a linear polarizer followed by a quarter-wavelength plate as shown in Fig. 4.

In the coherent radiation emission experiments, essentially the same system was used except for the cell which was then made of quartz and placed inside a microwave cavity. The arrangement is shown in Fig. 6. The quartz cells have a 2-cm diameter and a length of about 1 cm. The cavity is made of brass and is operated in the TE_{011} mode. The loaded cavity Q, with an external coupling of 1 (match condition) is 3000. A hole is made on the side of the cavity to allow observation of fluorescence. The laser beam has a diameter of 18 mm and enters into the cavity through a copper metal mesh. The coherent microwave radiation emission is detected with a spectrum analyzer that can be operated both in the frequency domain to observe the spectrum of emission and in the time domain to make measurements on the line shape of the emitted radiation and on the transient behavior of the atomic ensemble.

TABLE I. Relative amplitudes of the dark lines shown in Fig. 7 in a cesium cell without buffer gas. The results are compared to those calculated from Clebsch-Gordan coefficients.

Transition (ground state)	$-3-3$	$-2-2$	$-1-1$	00	11	22	33
Calculated	1.06	1.21	1.16	1	0.78	0.49	0.27
Experiment	0.89	1.22	1.11	1	0.72	0.44	0.33

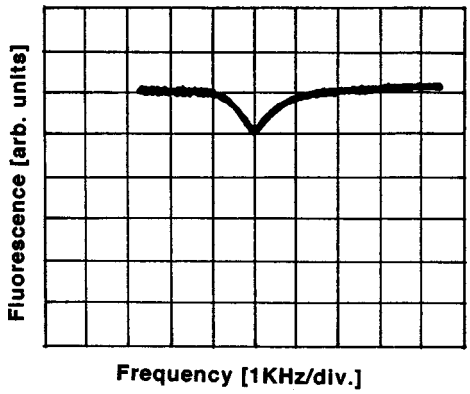

FIG. 8. Dark line observed for the Cs O-O transition in the case of methane is used as buffer gas; the methane pressure was 9 Torr and the temperature was 20 °C; $\Gamma' \sim \gamma_2$.

B. The Cs dark lines

Total spectrum. The $\Delta m=0$ dark lines of cesium were observed directly by using the system of Fig. 4 and by sweeping the frequency of the synthesizer over a range of frequencies covering the whole spectrum. The fluorescence signal observed in a cell without buffer gas is shown in Fig. 7 for the case when the laser frequency is adjusted such as to excite transitions between the ground levels and the $P_{3/2}$, $F=4$ level. The linewidth is determined essentially by the transit time of the atoms across the laser beam and is of the order of 100 kHz. The relative amplitude of the seven dark lines reflects directly the amplitude of the transition probabilities from the ground levels to the $P_{3/2}$ state. This was verified through a calculation using Clebsch-Gordan coefficients. The results are reported in Table I. Similar results were obtained with both signs of circular polarization, σ^+ or σ^-, as well as for transitions to the $P_{3/2}$, $F=3$ state.

O-O transitions. A Cs O-O dark line as observed with the system of Fig. 4 and a cell containing methane as a buffer gas at a temperature of 20 °C is shown in Fig. 8. The contrast was about 1.5%, with $\Gamma' \sim \gamma_2$, a value that agrees with calculations taking into account the fluorescence originating from all allowed transitions and the presence of the buffer gas mixing the excited states. This result is reported in Table II with that obtained for the case where the cell does not contain a buffer gas for the case $\Gamma' \gg \gamma_2$.

The linewidth at half the height of the O-O transition was measured for several cells containing various buffer gases. This was done as a function of laser power, the result are shown in Table III with other data of interest on the properties of the cells. The narrowest linewidth is obtained with neon at a pressure of 46 Torr and is about 50 Hz. This is in

TABLE II. Dark line contrast, calculated and observed for the O-O transition in cesium in the case of cells with or without buffer gases.

	Calculation	Experiment
Contrast	O-O transition	
No buffer gas	6.2%	5%
Buffer gas	3.1%	2 to 3%

TABLE III. Optical and microwave line widths studied in the dark line experiments with the cylindrical cells (4×4 cm); (1) calculated from natural lifetime; (2) calculated from experimental data and using a Voigt profile; (3) limit extrapolated to zero power broadening; (4) measured with the free induction decay.

Buffer gas	P (Torr)	$\Delta\nu_{op}$ (MHz)	$\Gamma^*/2\pi$ (MHz)	γ_2/π (Hz)$^{(3)}$
None		528	5 (1)	
Ne	45.8	962	690 (2)	56[a]
Ne	37.4			47 (4)
CH_4	9.3	840	490 (2)	268
CH_4	17.5	980	720 (2)	244
C_3H_8	19.7	962	690 (2)	407
C_4H_{10}	11.5	927	650 (2)	397
N_2	19.0			80 (4)

*See also Ref. [23].

agreement with the results reported by Brandt *et al.* [23]. The widths reported are values obtained at room temperature and extrapolated to zero laser intensity. The laser intensity may be varied both through attenuation of intensity with neutral density filters or by expansion of the beam. This last method has advantages since an increase in beam diameter increases the number of atoms in interaction. The results for the case of nitrogen are shown in Fig. 9.

The width of the dark line, as given by Eq. (1), may be written as

$$\Delta\nu_{1/2}=(1/\pi)(\gamma_2+\Gamma'). \tag{60}$$

In a cylindrical cell of length l and diameter a, containing a buffer gas at pressure P, γ_2 is given by [15]:

$$\gamma_2=\{(2.4/a)^2+(\pi/l)^2\}D_0(P_0/P) + L_0\overline{v_{rbg}}g\sigma_{2bg}(P/P_0)+\gamma_{2se}, \tag{61}$$

where D_0 is the diffusion constant of the cesium atoms in the buffer gas, P_0 corresponds to one atmosphere, L_0 is the Loschmidt constant, $\overline{v_{rbg}}$ is the average relative velocity of the cesium and buffer gas atoms, σ_{2bg} is the cesium–buffer gas collision cross section and γ_{2se} is the coherence spin exchange relaxation rate. At moderate pressures ($>$ 10 to 20 Torr depending on the buffer gas), diffusion to the walls of the cell does not contribute much to relaxation. The first term between brackets in Eq. (61) becomes negligible in comparison to the second term, the cesium–buffer gas collision relaxation rate. At high temperatures, of the order of 50 °C, the density of cesium is such as to make spin exchange relaxation predominant.

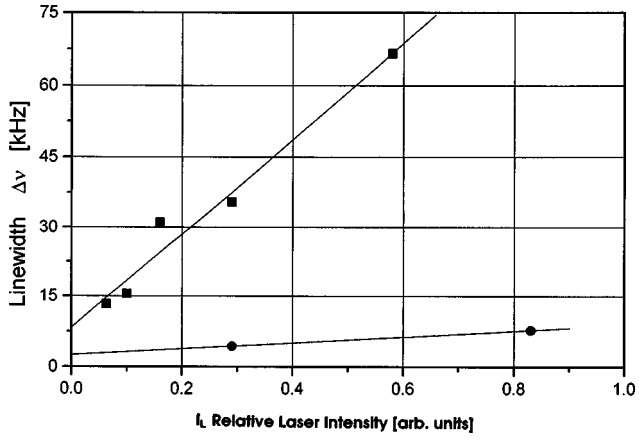

FIG. 9. Line width at half the height of the O-O transition in cesium in a cell containing nitrogen at a pressure of 7.4 Torr, at room temperature, as a function of laser power, for two different sizes of cross section of laser beam: ■, 2 mm^2; ●, 80 mm^2.

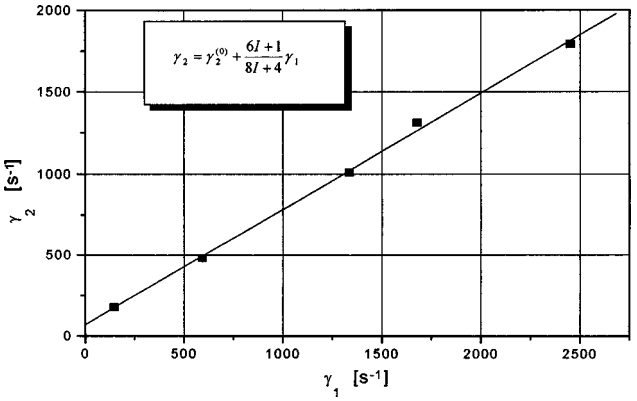

FIG. 10. Experimental data on spin exchange relaxation rates. The value of γ_2 is plotted against the value γ_1 as measured by the free induction decay.

Spin exchange relaxation. The coherence spin exchange relaxation rate is given by [15]

$$\gamma_{2se}=Rn\overline{v_r}\sigma_{se} \tag{62}$$

and the population relaxation rate γ_{1se} by

$$\gamma_{1se}=n\overline{v_r}\sigma_{se}. \tag{63}$$

Here, n is the cesium density, $\overline{v_r}$ is the average relative velocity of the cesium atoms, σ_{se} is the cesium spin exchange cross section equal to 2.18×10^{-14} cm^2 and R is a factor derived from the basic spin exchange process for a manifold of hyperfine levels. It is equal to [24,15]

$$R=\frac{6I+1}{8I+4}, \tag{64}$$

where I is the nuclear spin. R gives the ratio of γ_2/γ_1 in spin exchange processes. In the case of cesium, $I=\frac{7}{2}$ and R is equal to 0.687. This relation has been verified in the case of rubidium and hydrogen and found to be in agreement with experimental data [18,25,26]. We have verified it in the present case. The results are shown in Fig. 10 as a plot of γ_1 against γ_2. The technique avoids the requirement of determining the actual density of cesium in the cell which is a rather inaccurate operation. The measurements were done with the system shown in Fig. 6 in which intensity optical pumping was used. In this case the laser was operated without microwave modulation, its frequency tuned to the $S_{1/2}$, $F=3$ to $P_{3/2}$ transition. It was pulsed by means of the acousto-optic modulator. This laser pulse, causing an inversion of population, was followed by a $\pi/2$ microwave pulse at 9.2 GHz, and the delayed pulse technique described in Ref. [18] was used to obtain values of γ_2 and γ_1 as a func-

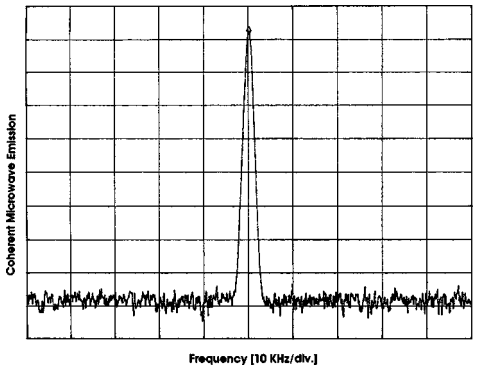

FIG. 11. Spectrum of the coherent emission of microwave radiation in the case of a cell containing nitrogen at a pressure of 19 Torr. Power at the peak, 140 fW; vertical axis, 5 dB/div.; central frequency, 9 192 651 130 Hz; resolution bandwidth, 1 kHz; video bandwidth, 1 kHz.

tion of the cesium density that was controlled by the cell temperature. It is observed that the experimental data is in agreement with Eqs. (62)–(64) within experimental errors.

C. Coherent microwave emission

1. Continuous operation

The experimental arrangement of Fig. 6 was used to measure the coherent microwave radiation emitted by the cesium atoms when driven into a coherent state by the laser sidebands in the Λ scheme. A typical spectrum is shown in Fig. 11 for the field-independent O-O transition with the cell containing nitrogen at a pressure of 19 Torr and the laser intensity adjusted to have Γ' approximately equal to $10\gamma_2$. The temperature was 48 °C. The emission takes place at twice the laser modulation frequency. The power output is 1.4×10^{-13} W and the signal to noise ratio is 10^4 with a resolution bandwidth of 1 kHz. The spectral profile of the emission can also be observed by scanning the laser modulation frequency over the width of the emission. The result is shown for the same cell in Fig. 12; the emission profile is Lorentzian in agreement with Eq. (42) and is centered at $\omega_{\mu'\mu}$, taking into account the second-order Zeeman shift and the buffer gas shift. The emitted power can be calculated

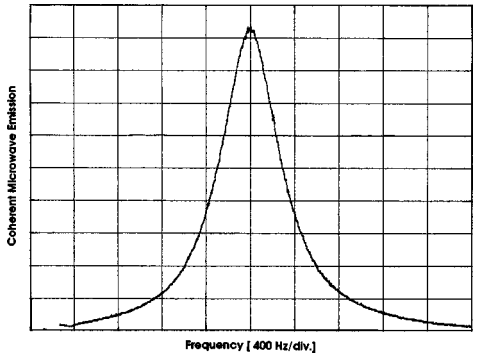

FIG. 12. Spectral profile of the coherent emission. The buffer gas is nitrogen at a pressure of 19 Torr and the cell temperature is 45 °C; central frequency, 9 192 651 GHz; resolution bandwidth, 3 kHz; video bandwidth, 3 kHz. The power at the peak is 60 fW; $\Gamma' \sim 3\gamma_2$.

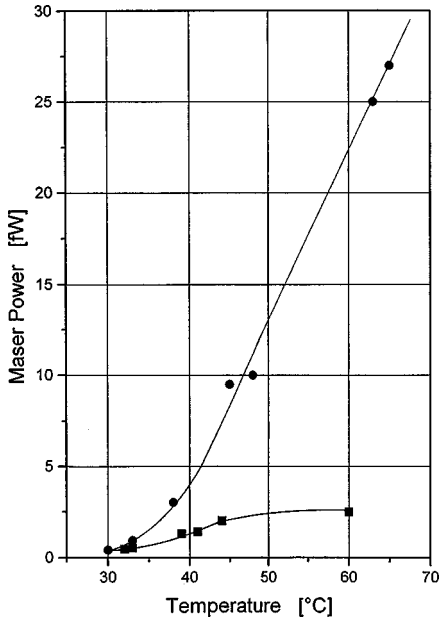

FIG. 13. Power output as a function of temperature for the cases when neon (■) (37 Torr) and nitrogen (●)(19 Torr) are used as buffer gases. The laser beam diameter is 6 mm.

with the help of Eqs. (42) and (43). The density is obtained from the contribution of spin exchange relaxation to the rate γ_2. The value of Γ' is obtained from the broadening of the emission line or the buildup rate. The volume of the atoms in interaction is evaluated from the size of the cell and the diameter of the laser beam. It is also realized that only those atoms in levels $m_F = 0$ contribute to the emission. The filling factor, evaluated from geometry, is approximately 0.2. With a loaded Q of 3000 and a coupling of 1, we obtain

$$k \sim 20\ \mathrm{s}^{-1}.$$

With a cavity coupling coefficient $\beta = 1$, and a cable loss of 3 dB we finally obtain

$$P_{\mathrm{out}} \sim 3 \times 10^{-13}\ \mathrm{W},$$

which is of the order of magnitude of the power observed in the experiment. The value of δ^r can also be calculated from the transverse pumping rate and the coherence relaxation rate. Using Eq. (57) it is then possible to evaluate the Rabi frequency b. It is of the order of 15 s^{-1}, thus rather small. This justifies the approach used in the perturbation analysis in which the coherence created by the laser was treated independently of the effect of the rf field on the density matrix elements.

The power output was also measured as a function of cell temperature. The results are shown in Fig. 13 for two cells containing nitrogen (19 Torr) and neon (37 Torr). The power emitted by the cell containing nitrogen increases with temperature while that containing neon appears to reach a maximum at a temperature above 45 °C. This behavior is believed to be due to the property of the nitrogen buffer gas in quenching the fluorescence radiation [27]. In the case of neon, the fluorescence emitted by the cesium atoms excites transitions in the ensemble and causes a loss of optical coherence. The fluorescence is said to optically pump the sys-

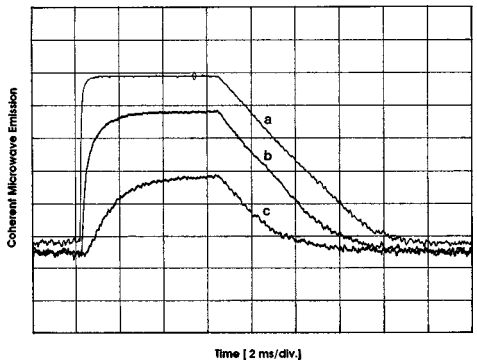

FIG. 14. Output power as measured in the transient mode for three laser intensities. Buffer gas, nitrogen at 19 Torr; cell temperature, 45 °C. (a) $\Gamma' \sim 10\gamma_2$, $P_0 = 90$ fW, $\tau_p = 0.2$ ms. (b) $\Gamma' \sim \gamma_2$, $P_0 = 30$ fW, $\tau_p = 1.0$ ms. (c) $\Gamma' \sim 0.2\gamma_2$, $P_0 = 3$ fW, $\tau_p = 1.7$ ms. Vertical axis, 5 dB/div.; lF bandwidth, 10 kHz; video bandwidth, 10 kHz. The free decay time constant is 1 ms.

tem in a random way. With nitrogen the fluorescence is reduced by several orders of magnitude and there is a reduced loss of coherence due to this effect.

2. Transient operation

Emission of microwave radiation for the laser operated under pulse mode gives information on the atomic system parameters. A typical result is shown in Fig. 14 for three laser intensities for the case in which nitrogen is used as the buffer gas. In that experiment the laser pulse was 6 ms long and its rise time and fall time were of the order of 1 μs, thus completely negligible in comparison to the decay times and the buildup times of the coherence. The three regions identified in the theoretical analysis are clearly visible. In that figure, the sidebands are tuned to the optical transition while the microwave angular frequency is tuned to the hyperfine angular frequency $\omega_{\mu'\mu}$.

Figure 15(a) shows the detailed emission behavior at the beginning of the laser pulse for the case when the microwave angular frequency is detuned from the resonant angular frequency $\omega_{\mu'\mu}$ by $\Omega_\mu = 2\pi \times 2$ kHz. The ringing is clearly visible. Its frequency is the difference between the microwave and the hyperfine resonance frequency as predicted by theory. Furthermore, this ringing disappears when the steady-state emission is reached towards the end of the laser pulse. In that region the emission frequency is that of the difference frequency ω_{21} between the sidebands. Figure 15(b) is a computer simulation using Eq. (49) for the same situation as that shown in Fig. 15(a). It is in agreement with the general behavior of the experimental observation.

The power buildup time is related to $\tau_p = 1/(\gamma_2 + \omega_R^2/\Gamma^*)$ [see Eq. (49)] and once γ_2 is evaluated from measurements on the decay time the transverse pumping rate Γ' can be determined. It is found experimentally that optimum signals (amplitude versus linewidth) are obtained with Γ' approximately equal to γ_2. After the laser pulse, the emission of power decays at the rate $2\gamma_2$ and gives a means of measuring γ_2. In that case γ_2 is of the order of 500 s^{-1}.

Figure 16 shows the spectrum of the microwave emission when the laser is switched on and off for equal periods of 30 ms, a period much longer than the characteristic times in-

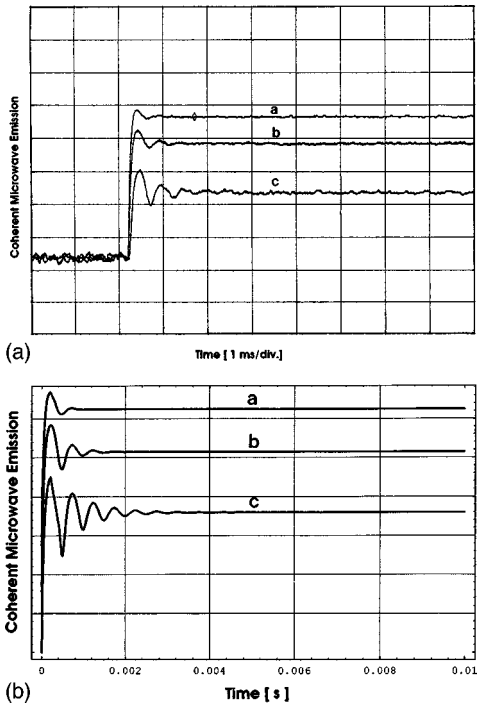

FIG. 15. (a) Behavior of the coherent microwave emission at the beginning of the laser pulse for three laser intensities when $\Omega_\mu = 2\pi \times 2.0$ kHz. (a) $\Gamma' = 10\gamma_2$; (b) $\Gamma' = 5\gamma_2$; (c) $\Gamma' = 2\gamma_2$. Buffer gas is nitrogen at 19 Torr and cell temperature is 45 °C. Vertical axis, 5 dB/div. (b) Computer simulation of Eq. (49) for the same situation as in (a). Vertical axis: 5 dB/div.

volved in the CPT process. The coherent emission is observed at the frequency $(\omega_2 - \omega_1)/2\pi$ together with the spectrum due to the free decay of the magnetization, which is centered on the hyperfine frequency $\omega_{\mu'\mu}/2\pi$; its width is ~ 200 Hz$\sim \gamma_2/\pi$.

IV. APPLICATION TO ATOMIC FREQUENCY STANDARDS

A. Frequency locking systems and frequency stability

Both the dark line and the coherent microwave emission can be used for the implementation of an atomic frequency standard. In both cases, the frequency microwave generator

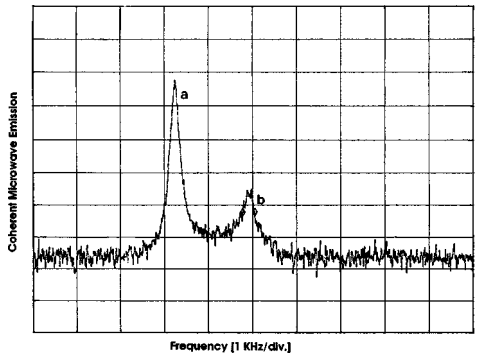

FIG. 16. RF spectrum of the coherent emission (a) and of the free decay (b) of the magnetization. Vertical axis, 5 dB/div.; resolution bandwidth, 100 Hz. Buffer gas is nitrogen at 19 Torr and cell temperature is 45 °C. $\Omega_\mu/2\pi = 1.6$ kHz.

used to modulate the laser frequency and create the coherent population trapping can be locked to the hyperfine resonance frequency. In the case of the dark line the locking is done to the maximum of the resonance line observed while in the case of microwave emission the locking is done at the maximum of power emitted. Systems have been constructed for achieving these locking and results are published elsewhere [28]. For example, in the case of a bench system locking a crystal oscillator to the coherent emission of radiation, a frequency stability of the order of 5×10^{-12} was observed over an averaging time of 100 s. Similar results were obtained in the case of the dark line. These are very promising results considering that the systems used were opened to environmental fluctuations.

B. Frequency shifts

In the realization of a frequency standard, attention must be paid to the various frequency shifts present in the ensemble, which, if not properly controlled, can affect the frequency stability of the standard. In the systems described above, the hyperfine frequency is perturbed by several phenomena. The frequency of the O-O transition is given by

$$\nu(\text{O-O})=\nu_{\text{Cs}}+\Delta\nu_B+\Delta\nu_{\text{bg}}+\Delta\nu_{\text{LS}}, \tag{65}$$

where ν_{Cs} as given by the definition of the time unit, is 9 192 631 770 Hz, $\Delta\nu_B$ is the magnetic field shift, $\Delta\nu_{\text{bg}}$ is the shift created by collisions between the buffer gas and the cesium atoms and $\Delta\nu_{\text{LS}}$ is the light shift.

Magnetic field shift. The O-O transition is affected by the magnetic field only in second order. A calculation using the Breit-Rabi formula gives a shift equal to [15]

$$\Delta\nu_B=427.45\times10^8 B_0^2 \tag{66}$$

where B_0 is expressed in Tesla. In the experiments described above the field was of the order of 4×10^{-5} T (400 mg) and the frequency shift was of the order of 70 Hz. This was done in order to counteract small residual field inhomogeneities and to obtain well-resolved resonance lines. In practice with a properly designed and well-shielded system a much smaller field can be used.

Buffer gas shift. The shift caused by collisions with the buffer gas is given by [15]

$$\Delta\nu_{\text{bg}}=P_0[\beta_0+\delta_0(T-T_0)+\gamma_0(T-T_0)^2], \tag{67}$$

where P_0 is the buffer gas pressure, β_0 is the pressure shift coefficient, δ_0 and γ_0 are the first- and second-order temperature coefficients, respectively, and T is the temperature of the ensemble of atoms. The temperature T_0 is the reference temperature at which the coefficients are measured. The pressure shifts and temperature coefficients may be negative or positive depending on the buffer gas used. In the experiments on the dark line, the cells contained the following buffer gases: nitrogen, neon, methane, and several other buffer gases in the C_nH_{2n+2} group. Measurements of the various coefficients have been reported by Beverini, Strumia, and Rovera [22]. The buffer gas pressure in all cells was of the order of tens of Torr causing frequency shifts of the order of a few kHz. These frequency shifts were measured in all cells and found to agree with the published data within experimental errors. In practice, in the case of the implementation of practical frequency standards using buffer gases, a mixture of these buffer gas is used to reduce the temperature coefficient. This technique can also be used in the present systems.

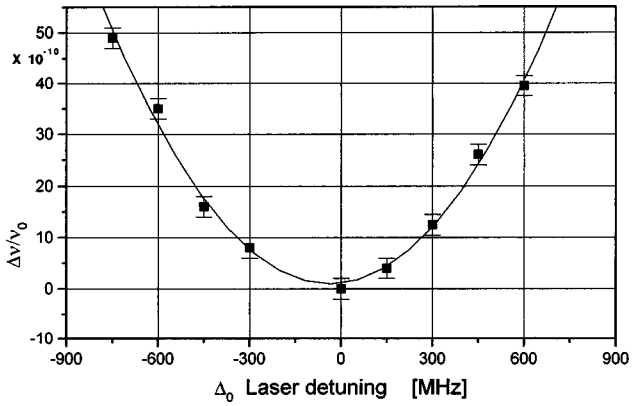

FIG. 17. Fractional frequency shift of the coherent microwave emission peak vs laser detuning Δ_0. The buffer gas is nitrogen at 19 Torr and the cell temperature is 45 °C. Laser power is such as to have $\Gamma'=\gamma_2$.

Light shift. The light shift is an effect that appears when the laser frequency is detuned from the central frequency of the optical transitions [29]. In the calculation we have assumed that the two sidebands have equal amplitudes. If we remove this condition and solve Equations (11)–(13) as we did before, we find that the dark line and the coherent emission central frequency is shifted by

$$\Delta\omega_{\text{LS}}=-\frac{1}{4}\left(\frac{\Delta_0}{(\Gamma^*/2)^2+\Delta_0^2}\right)[\omega_{1R}^2-\omega_{2R}^2], \tag{68}$$

where it is assumed that the two lasers are detuned from the optical resonances by the same quantity Δ_0. As was described above, a single laser modulated at a subharmonic of the hyperfine frequency was used throughout the experiments to create the two coherent radiations required in the observation of the CPT phenomenon. In such a case, a detuning of the laser causes an equal frequency shift of the two sidebands. It is readily observed that if the two laser radiations have equal amplitude, the optical Rabi frequencies are equal and the light shift vanishes. This is intuitively expected since in such a situation the interference property inherent to CPT prevents excitation of atoms to the P state. Since no excitations take place there is no light shift.

We have measured the frequency of the coherent microwave emission peak as a function of the detuning of the laser central frequency. For this experiment, the microwave frequency was locked to the maximum of the emission by means of standard servo loop techniques [28] and the laser frequency was varied by adjusting the injection current. The laser sidebands were equal within experimental error. The results are shown in Fig. 17. It is observed that the first-order light shift is absent as expected from Eq. (68). Other experiments made in situations where the sidebands amplitude were different by a factor of the order of ten showed the presence of a large linear light shift. In the present case, however, a small residual second-order frequency shift is

present. It may be due to second-order effects that are not taken into account in the first-order perturbation approach developed above, such as the presence of a residual carrier and the presence of other sidebands in the laser spectrum.

Cavity pulling in the coherent microwave emission approach. The effect of the cavity tuning on the frequency of the coherent microwave emission can be calculated from Eq. (42) in the limit of $b \ll \Delta\omega_{1/2}$. The amplitude of the power output is function of the cavity frequency tuning. Consequently a technique that locks the frequency of the microwave generator to the maximum of emission will be affected by the cavity tuning. The effect can be calculated by differentiating Eq. (42) with respect to ω_{21} to obtain the maximum of emission. The maximum appears at $\omega_{21\,\max}$ for the condition

$$(\omega_{21\,\max}-\omega_{\mu'\mu})=\left(\frac{Q_L}{Q_{\rm at}}\right)^2(\omega_{21\,\max}-\omega_c), \qquad (69)$$

where $Q_{\rm at}$ is the resonance line quality factor defined as $(\omega_{\mu'\mu}/2\pi\Delta\nu_{1/2})$. The frequency at the maximum of emission is thus displaced by a cavity detuning. However, the apparent frequency shift caused by the cavity detuning is attenuated by the square of the ratio of the loaded cavity Q_L to the atomic line $Q_{\rm at}$. In the present setup this ratio is of the order of 10^{-4}. The attenuation is thus 10^8, making the effect negligible. Other frequency shifts such as the spin exchange frequency shift and the Bloch-Siegert effect are negligible in comparison to the buffer gas and magnetic frequency shifts [15].

V. CONCLUSION

In the present paper we have used a perturbation analysis to obtain transparent analytical expressions for the phenomenon of coherent population trapping. We have obtained a simple expression for the dark line and we have shown that in the case of alkali atoms such as cesium, CPT leads to the emission of coherent microwave radiation at the hyperfine frequency, easily detected with the help of a microwave cavity. This phenomenon could be interpreted as stimulated coherent Raman emission at the ground state hyperfine frequency. The resulting device may also be said to belong to the group of atomic oscillators such as the hydrogen and the rubidium masers [30,31]. Experiments were reported that confirm the results of the theoretical analysis.

Both phenomena, the dark line and the coherent microwave emission, can be used for the implementation of a frequency standard with interesting characteristics. In particular, the problem of frequency multiplication inherent in the standard intensity optical pumping approach is relaxed through direct frequency multiplication in the laser diode. There is no first-order light shift. In the case of the dark line there is no cavity required for excitation at the hyperfine frequency. Finally, in the case of coherent microwave emission, the cavity pulling is reduced to a negligible value.

This work could be extended to the cases of rubidium 85 (3.04 GHz) and rubidium 87 (6.83 GHz). Future experiments could be oriented towards a better understanding of the light shift and towards the practical implementation of a frequency standard based on either effects, the dark line or the coherent emission of microwave radiation.

ACKNOWLEDGMENTS

The authors wish to thank C. Novero, P. Tavella, N. Beverini, F. Strumia, D. Andreone, A. De Marchi, F. Bertinetto, M. Inguscio, E. Arimondo, and S. Leschiutta for their collaboration, help, and encouragement at various stages of this work. This work was partially supported by the Italian Space Agency (ASI).

[1] G. Alzetta, A. Gozzini, L. Moi, and G. Orriols, Nuovo Cimento B **36**, 5 (1976).
[2] G. Orriols, Nuovo Cimento **53**, 1 (1979).
[3] E. Arimondo, Prog. Opt. **XXXV**, 257 (1996).
[4] A. Aspect, E. Arimondo, R. Kaiser, N. Vansteenkiste, and C. Cohen-Tannoudji, J. Opt. Soc. Am. B **11**, 2112 (1989).
[5] M. O. Scully and M. Fleischauer, Phys. Rev. Lett. **69**, 1360 (1992).
[6] M. O. Scully, Phys. Rep. **219**, 191 (1992).
[7] N. Cyr, M. Têtu, and M. Breton, IEEE Trans Instrum. Meas. **42**, 640 (1993).
[8] A. S. Zibrov, H. G. Robinson, V. L. Velichansky, V. V. Vasiliev, L. Holberg, E. Arimondo, M. D. Lukin and M. O. Scully, in *Proceedings of the 5th Symposium on Frequency Standards & Metrology*, edited by J. C. Bergquist (World Scientific, Singapore, 1995), p. 490.
[9] F. Levi, A. Godone, C. Novero, and J. Vanier, *Proceedings of the 11th European Frequency and Time Forum, Neuchâtel, Switzerland, 1997* (unpublished).
[10] A. Godone, F. Levi, and J. Vanier (unpublished).
[11] A. M. Akulshin, A. A. Celikov, and V. L. Velichansky, Opt. Commun. **84**, 139 (1991).
[12] R. H. Dicke, Phys. Rev. **89**, 472 (1953).
[13] C. P. Slichter, *Principles of Magnetic Resonance* (Harper and Row, New York, 1963).
[14] See, for example, R. G. Brewer and E. L. Hahn, Phys. Rev. A **11**, 1641 (1975), and the review by E. Arimondo, Prog. Opt. **XXXV**, 257 (1996).
[15] J. Vanier and C. Audoin, *The Quantum Physics of Atomic Frequency Standards* (Adam Hilger, Bristol, England, 1989).
[16] S. Bloom, J. Appl. Phys. **27**, 785 (1956).
[17] J. Vanier, Phys. Rev. Lett. **18**, 33 (1967).
[18] J. Vanier, Phys. Rev. **168**, 129 (1968).
[19] C. J. Myatt, N. R. Newbury, and C. Wieman, Opt. Lett. **18**, 8 (1993).
[20] S. Kobayashi, Y. Yamamoto, M. Ito, and T. Kimura, IEEE J. Quantum Electron. **18**, 4 (1982).
[21] G. Rovera, A. De Marchi, and J. Vanier, IEEE Trans. Instrum. Meas. **3**, 203 (1976).
[22] N. Beverini, F. Strumia, and G. Rovera, Opt. Commun. **37**, 394 (1981).

[23] S. Brandt, A. Nagel, R. Wynands, and D. Meschede, Phys. Rev. A **56**, 2 (1997); **56**, 1063 (1997).
[24] F. Grossetête, J. Phys. (Paris) **29**, 456 (1968).
[25] J. Vanier, J. S. Boulanger, and J. F. Simard, Phys. Rev. A **9**, 1031 (1974).
[26] J. Vanier, R. Brousseau, and R. Larouche, Can. J. Phys. **51**, 1901 (1973).
[27] W. Happer, Rev. Mod. Phys. **44**, 169 (1972).
[28] A. Godone, F. Levi, and J. Vanier (unpublished).
[29] J. P. Barrat and C. Cohen-Tannoudji, J. Phys. Radium **22**, 329 (1961).
[30] D. Kleppner, H. M. Goldenberg, and N. F. Ramsey, Phys. Rev. **126**, 603 (1962).
[31] P. Davidovits, Appl. Phys. Lett. **5**, 15 (1964).